

ON THE STRUCTURAL PROPERTIES OF FLASH- EVAPORATED THIN FILM GALLIUM ARSENIDE WITH THE PRESENCE OF TIN VAPOR DURING GROWTH

DING HUA HU

College of Engineering National Chiao Tung University

(Received 12, October 1971)

Abstract—*Structural analysis of x-ray diffraction peaks for flash-evaporated GaAs thin films has shown that the crystalline size is enhanced by the presence of tin vapor pressure during growth. This phenomenon can be related to the regrown process as the tin moves from the bulk to the outer growth surface. The forcing mechanism for tin movement is a temperature gradient.*

I. INTRODUCTION

The large difference in the vapor pressure of gallium and arsenic has hampered the growth of stoichiometric GaAs films by vacuum evaporation. Experimentally it has been found that the sticking coefficient of As is substantially less than that of Ga, except when the As strikes the Ga surface¹. This may lead to a Ga-rich film even for a source vapor beam of stoichiometric ratio of Ga and As. It has been suggested that the stoichiometry of the films could be best controlled by the larger than 1:1 ratio of arsenic to gallium for the source vapor beam and the use of a high substrate temperature². The result would be that no excess gallium atoms could accumulate in the condensed film. Since there is no stable alloy phase near the composition GaAs, the excess arsenic is likely to be lost from the deposit fairly readily. Moreover, a high substrate temperature has the advantage of favoring larger crystallite sizes, fewer imperfections, less adsorbed and condensed foreign atoms, and less possibility of forming the metastable wurtzite phase^{3,4}. However, it is doubtful that a good *n*-type GaAs film could be obtained when the addition of tin vapor pressure is introduced, because of the possible formation of Sn₃As₂. The present work is to investigate the influence of the tin vapor pressure on the structural properties of flash-evaporated thin films GaAs.

II. FILM PREPARATION

The evaporation system is shown in Figure 1. The main boat was maintained at 1500°C (measured by optical pyrometer) during the evaporation. The tin dopant boat temperature was varied over a range of 800°C to 1000°C. Prior to deposition, the vacuum system was pumped down to 10⁻⁶ Torr; depositions were carried out at 5×10⁻⁵ Torr.

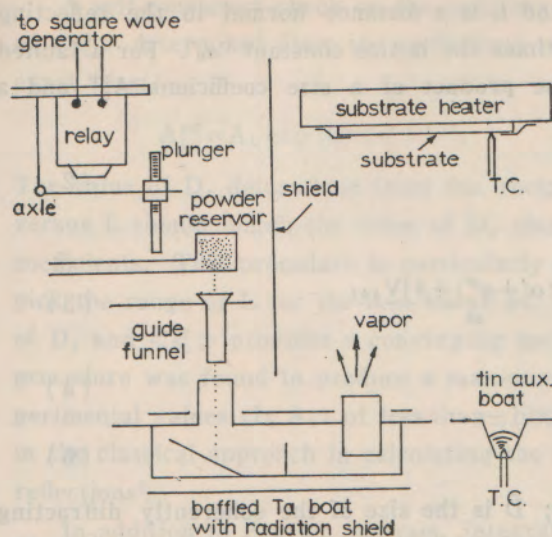


Fig. 1. Schematic Representation of the Flash-Evaporation System.

A closed and shielded tantalum boat with an inlet and an outlet was used for the evaporator. The boat had a 22.5° angle surface and baffles inside to deflect the bouncing grain, until complete evaporation was accomplished. The tin dopant boat was made of molybdenum wire, wound into a conical shape and coated with alumina. The substrates used were Corning 0215 glass or Corning 7059 glass. The substrate heater was made from molybdenum sheet.

Mixtures of high purity GaAs polycrystalline powders with As powders were fed continuously from

the powder feeder into the main boat. In this work the SEVAC grade GaAs powders (from SEMI-ELEMENTS) was ground and sieved. Only the size range $66\ \mu$ to $88\ \mu$ was used. The feeder mechanism allowed precise control of the powder feed from very slow to rapid delivery rates. A guide funnel was used to limit the amount of GaAs powder which would be diverted by back streaming vapor. A shield between the guide funnel and substrate prevented the volatile arsenous oxide (As_2O_3), which evaporates from the As immediately on entering the funnel, from condensing on the substrate.

III. DETERMINATION OF STRUCTURE PARAMETERS

X-ray diffraction analysis was used to determine the bulk structure of flash-evaporated thin GaAs film deposited on amorphous glass substrate. The flat geometry of the samples necessitated the use of a diffractometer. A least-squares polynomial approximation⁵ of the Warren-Averbach method was employed to analyze single peaks. Integral breadth measurements are discussed for comparison. Peak shifts and peak asymmetry were used to study faulting and density change. Imperfections in the crystallites have a major effect on the diffraction patterns of these films. Strain and small crystallite size broaden the profiles, while stacking faults and twinning make the profiles asymmetrical. The shifts in the peaks of a powder pattern can be related to density changes, mean strain, and stacking faults.

The profile $P(S)$ or $P(2\theta)$ of a powder pattern peak, corrected for instrumental broadening can be expressed as a Fourier series⁶⁻⁸:

$$P(S) = \sum_{-\infty}^{+\infty} [A_L \cos 2\pi L(S - S_0) + B_L \sin 2\pi L(S - S_0)] \quad (1)$$

where $S = (2 \sin \theta) / \lambda$, $S_0 = (2 \sin \theta_0) / \lambda$

is the position of the peak maximum and L is a distance normal to the reflecting plane (hkl) and equal to the order n times the lattice constant " a_0 ". For a faulted material, the cosine coefficient A_L is the product of a size coefficient A_L^{PF} and a distortion coefficient A_L^{PS} :

$$A_L = A_L^P \cdot A_L^D \tag{2}$$

For small values of L ,

$$A_L^{PF} = 1 - \frac{L}{D_e} = 1 - \frac{L}{D} + \frac{[1.5(\alpha' + \alpha'') + \beta]V_{hkl}}{a} \tag{3}$$

$$A_L^D = 1 - \frac{2\pi^2 L^2 \langle \epsilon_L^2 \rangle}{a^2} > h_0^2 \tag{4}$$

$$(h_0^2 = h^2 + k^2 + l^2) \tag{5}$$

where D_e is the effective particle size; \bar{D} is the size of the coherently diffracting domains in the direction normal to the reflecting planes (hkl); α' , α'' and β are the single, double deformation and twin fault probabilities, respectively and $\langle \epsilon_L^2 \rangle$ is the mean square strain component normal to the reflecting planes (hkl). The coefficient V_{hkl} for faulting on (111) plane in fcc material is given by

$$V_{hkl} = \frac{1}{(u+b)h_0} \sum |h+k+1| \tag{2}$$

The number of components of a powder pattern peak which are unaffected by faulting (i. e., $h+k+1=3N$, N being integer) is designated by " u " and the number of components which are broadened by the faults is " b " (i. e., $h+k+1=3N \pm 1$).

The Warren-Averbach⁶ method of separation of the particle size and strain coefficients involves a plot of $\ln A_L$ vs. h_0^2 for two or more orders of a reflection. However, if the material to be analyzed is elastically isotropic then all the reflections of the sample can be used in the separation plot⁹. The calculated value of the elastic anisotropic factor for bulk GaAs is 1.83 and hence the use of all the reflections of GaAs films in the W-A separation plot is not allowed.

The minimum particle size, $D_{min.}$, can be established by considering the extreme case in which all the broadening is due to small particle size (i. e., $A_L = A_L^{PF}$). In this case, $D_{min.}$ is calculated from the initial slope of the (A_L, L) curves and is complicated by the "hook effect"^{7,8} which causes an inaccuracy in the value of A_0 . An approximate correction for this effect is to completely ignore the A_0 and to use only the first few points to calculate the slope and $D_{min.}$

Equation (2) can be expanded for small values of L and $\langle \epsilon_L^2 \rangle$ as

$$A_L = 1 - \frac{L}{D_e} - C^2 \langle \epsilon_L^2 \rangle L^2 + \frac{C^2 \langle \epsilon_L^2 \rangle L^3}{D_e} \tag{7}$$

Where $C^2 = 2(h_0/a)^2$. By representing this equation with a third order polynomial in L , using a least-squares fit, D_e and $\langle \epsilon_L^2 \rangle$ can be separately determined. In order to avoid "hook effect" and satisfy equation (7), only coefficients associated with the range $0.1 D_{min.} < L < D_{min.}$

A self-consistent check on the accuracy of the curve fitting is to use the value of $\langle \epsilon_L^2 \rangle$ determined from the coefficients to calculate A_L^{PF} from equation (2) in the exact form,

$$A_L^{PF} = A_L \exp(C^2 \langle \epsilon_L^2 \rangle L^2). \tag{8}$$

The value of D_e determined from the reciprocal of the initial slope of this A_L^{PF} versus L should match the value of D_e obtained from the least-squares fit of the coefficients. This procedure is particularly useful when the computer is allowed to pick the range of L for the best curve fit. If too many harmonics are used, values of D_e and $\langle \epsilon_L^2 \rangle$ provides a converging method for the iteration. This curve fitting procedure was found to produce a maximum error between the computed and experimental values (L, A_L) of less than $\pm 10\%$. A comparable error has been estimated in the classical approach in calculating the Fourier coefficients of the higher order reflections⁸.

In addition to Fourier analysis, integral breadth measurements of particle sizes were also evaluated. The integral breadth of a diffraction profile is defined as⁹:

$$B = \int_{(2\theta)_2}^{(2\theta)_1} P(2\theta) d(2\theta) / P_{\max}(2\theta) \tag{9}$$

where $P_{\max}(2\theta)$ is the maximum diffracted power per unit length. Wagner and Aqua¹⁰ have outlined the particular procedures required for instrumental broadening. To allow for data comparison, the three standard profile shapes, Cauchy, Gaussian, and Parabolic were used to calculate the effective particle size. In calculating the effective particle sizes for each assumed shape, the mean strain $\langle \epsilon \rangle$ was taken to be $1.25 \langle \epsilon_L^2 \rangle^{1/2}$ as was evaluated by Fourier methods¹⁰.

Stacking fault probability was determined from shifts in peak position maximum, using an internal silicon standard. The position of the peak maximum (PPM), (S_0), can be expressed as⁸:

$$S_0 = S_b - \langle \epsilon_L \rangle S_b - G_{hkl} \alpha S_b \tag{10}$$

with $S_b = \frac{2 \sin \theta_b}{\lambda} = \frac{1}{d_{hkl}^b}$ is the PPM of the broad reflection in the absence of strain and faults; $\langle \epsilon_L \rangle$ is the mean strain; $\alpha = \alpha' - \alpha''$ is the stacking fault probability; and,

$$G_{hkl} = \frac{-\sqrt{3}}{4\pi(u+b)} \sum_b \frac{\pm(h+k+l)}{h_0^2} \tag{11}$$

If S_a is the position of the peak maximum for the ideal peak (i.e., a sample with no strain, no faults, no density change and a large particle size) then the shift in peak position maximum is,

$$\Delta S = S_0 - S_a \sim \left(-\frac{\Delta a}{a} - \langle \epsilon_L \rangle - G_{hkl} \alpha \right) S_a \tag{12}$$

or
$$\Delta(2\theta^0)_{hkl} = -\frac{360}{\pi} \left(\frac{\Delta a}{a} + \langle \epsilon_L \rangle + G_{hkl} \alpha \right) \tan \theta_{hkl} \tag{13}$$

If mean strain is not a principal cause of the peak shift, equation (13) reduces to

$$\Delta(2\theta^0)_{hkl} = -\frac{360}{\pi} \left(\frac{\Delta a}{a} + G_{hkl} \alpha \right) \tan \theta_{hkl} \quad (14)$$

Simultaneous solution of equation (14) for peak position shift of the (311) and (220) plane allowed calculation of the stacking fault probability and the mean density change (or effective density change in case of strain).

The effective twin probability $\beta' = \beta + 4.5 \alpha''$ can be determined from the shift in the center of gravity of the diffraction profile¹¹. The shift in 2θ coordinates is given by,

$$\Delta C. G. (2\theta^0) = 2\theta_{v.c.g}^0 - 2\theta_{P.F.M}^0 = \frac{360 \ln 2}{\pi^2 \sqrt{3}} X_{hkl} (\beta + 4.5 \alpha'') \tan \theta_0 \quad (15)$$

$$X_{hkl} = \frac{1}{u+b} \sum_b \pm \frac{(h+k+l)}{|h+k+l|} \quad (16)$$

The X-ray diffraction unit consisted of a Phillips-Norelco wide-scan goniometer, a Picker copper X-ray tube, and Harshaw electronics for continuous recording of the intensities. The KB and white radiation were eliminated by a LiF crystal monochromator located in the diffracted beam. The minimum effective depth of beam penetration calculated for GaAs is larger than 25 microns. Since all the films grown in the laboratory for this investigation were less than a micron thick as measured with a micro-profilometer, it is safe to assume that the incident beam has penetrated the entire thickness of the film.

Fast scan of the sample was used for immediate identification of the material. Particle size estimates, abnormal line shape, and Bragg shift were obtained by detailed analysis of individual slow scans of the peaks. All diffraction peaks were corrected for instrumental broadening by the Stokes method¹⁵ using an annealed GaAs powder standard. Peak maxima were determined by the use of a silicon powder internal standard.

IV. RESULT AND DISCUSSION

Typical fast scan x-ray patterns of the tin doped GaAs films are shown in Figure 2. For a tin dopant temperature in excess of a critical temperature, extra peaks were detected. These extra reflections were compared to the reported d -spacings of tin arsenide, β -tin, and tin monoxide.¹² These are labeled in Figure 3. The tin monoxide peak can be detected only for films which are deposited under poor vacuum conditions (10^{-4} or poorer). It was found that these undesired surface layers could be etched off by dilute HCl. The most probable explanation for their formation is that during growth, excess tin and impurities are caused to move to the surface as a result of reaching the film's solubility limit or as a result of impurity segregation. Typical structure parameters are listed in Table 1, and will be interpreted in the following discussion. Films were grown with nearly the same boundary conditions while varying the amount of tin doping in increasing order. Substrate temperature was approximately 400°C and evaporation rate was approximately 400°C and evaporation rate was approximately 600 Å/min. A mixing ratio of As powder to GaAs powder was maintained at 1:1 by weight.

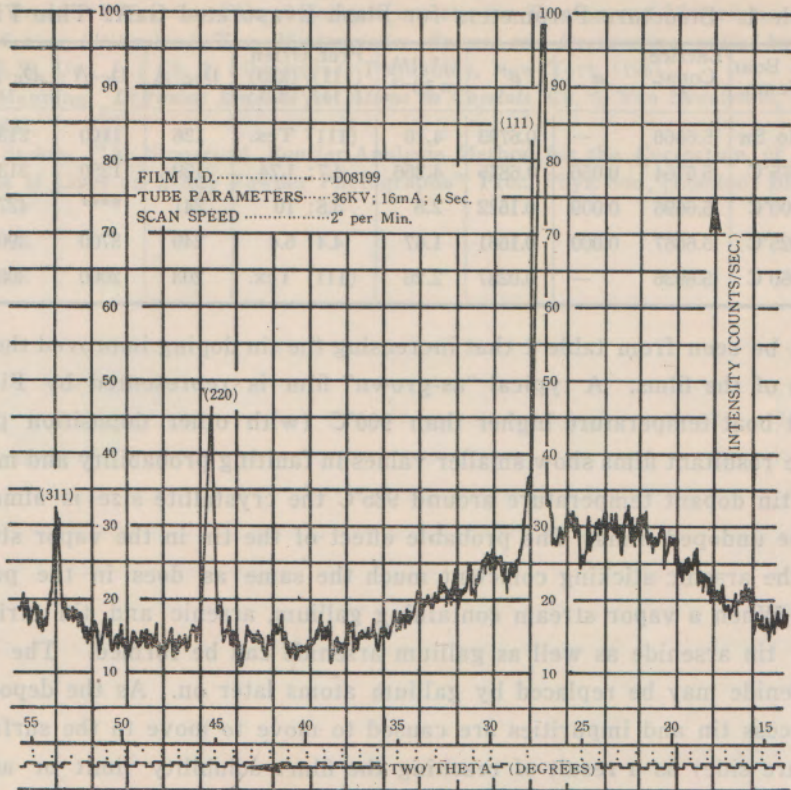


Fig. 2. Fast Scan of GaAs Film Deposited on Amorphous Glass Substrate.

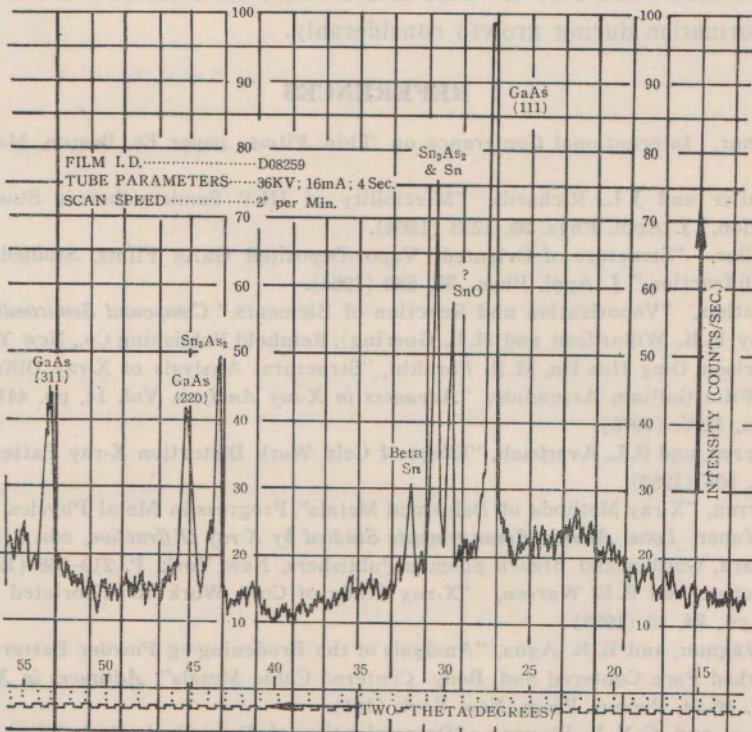


Fig. 3. East Scan of GaAs Film with Excessive Tin Vapor During Growth.

Table 1. Structure Parameters for Flash Evaporated GaAs Thin Films

Film	Sn Boat Temp.	Lattice Const. Å	α	β'	$(\epsilon_L^2)^{1/2} \times 10^{-3}$	Pref. Orient. (111)/(220) (111)/(311)	D_{FC} Å	D_C Å	D_G Å	D_{FA} Å
1	No Sn	5.6866	—	0.6793	4.10	(111) Tex.	126	1100	213	232
2	875°C	5.6764	0.056	0.6875	4.286	4.7; 1.74	129	1250	213	232
3	900°C	5.6696	0.009	0.1622	2.8	3.8; 10	241	****	427	610
4	925°C	5.6667	0.000	0.1661	1.67	4.4; 6.4	249	3700	390	487
5	950°C	5.6936	—	0.0287	2.26	(111) Tex.	203	2000	306	358

It can be seen from table 1 that increasing the tin doping improved the structure properties of the films. A typical "as-grown" film is represented by Film 1. For tin dopant boat temperature higher than 900°C (with other deposition parameters fixed), the resultant films show smaller values in faulting probability and microstrain. With the tin dopant temperature around 925°C the crystallite size is almost double that of the undoped films. The probable effect of the tin in the vapor stream is to increase the arsenic sticking coefficient much the same as does in the presence of gallium.¹ When a vapor stream containing gallium, arsenic and tin strikes a hot substrate, tin arsenide as well as gallium arsenide can be formed. The tin atoms in tin arsenide may be replaced by gallium atoms later on. As the deposition continues, excess tin and impurities are caused to move to the surface (lower temperature side) as a result of reaching the film's solubility limit or as a result of impurity segregation. These unwanted surface layers could be etched off by dilute HCl as mentioned before. This intermediate tin arsenide process would lower energy of formation during growth considerably.

REFERENCES

1. J. R. Arthur, International Conference on Thin Films, paper E6, Boston, Mass., April 29, 1969.
2. E. K. Muller and J. L. Richards, "Miscibility of III-V Semiconductors Studied by Flash Evaporation," *J. Appl. Phys.* **35**, 1233 (1964).
3. E. K. Muller, "Structure of Oriented, Vapor-Deposited GaAs Films, Studied by Electron Diffraction," *J. Appl. Phys.*, **35**, 580 (1964).
4. K. G. Gunther, "Vaporization and Reaction of Elements," *Compound Semiconductors*, Vol. 1, (edited by R. K. Willardson and H. L. Goering), Reinhold Publishing Co., New York (1962).
5. E. J. Charlson, Ding Hua Hu, M. R. Farukhi, "Structural Analysis of X-ray Diffraction Peaks of Thin Film Gallium Arsenide," *Advances in X-ray Analysis*, Vol. 14, pp. 441-452, Plenum Press Inc., N. Y. (1970).
6. B. E. Warren, and B. L. Averbach, "Effect of Cold Work Distortion X-ray Patterns," *J. Appl. Phys.*, **21**, 595 (1950).
7. B. E. Warren, "X-ray Methods of Deformed Metals", *Progress in Metal Physics*, **8**, 147 (1959).
8. C. N. J. Waner, *Local Atomic Arrangements Studied by X-ray Diffraction*, eds. J. B. Cohen and J. E. Hillard, Gordon and Breach Science Publishers, New York, P. 219-268 (1965).
9. M. Mckeehan, and B. E. Warren, "X-ray Study of Cold Work in Thoriated Tungsten," *J. Appl. Phys.*, **24**, 52 (1953).
10. C. N. J. Wagner, and E. N. Agua, "Analysis of the Broadening of Powder Pattern Peaks from Cold-Worked Face Centered and Body Centered Cubic Metals", *Advances in X-ray Analysis*, Vol. 7, P. 48-64, Plenum Press, New York (1964).
11. J. B. Cohen, and C. N. J. Wagner, "Determination of Twin Fault Probability from Diffraction Patterns of FCC Metals and Alloys", *J. Appl. Phys.*, **33**, 2073 (1962).

- 12. X-ray Powder Diffraction File, American society for Testing and Materials.
- 13. P. H. Sutter, "Diffusion," *The Moelectricity: Science and Engineering* (edited by R. R. Heikes and R. W. Ure, Jr.) Ch. 7, Interscience Publishers, New York (1961).
- 14. J. R. Manning, *Diffusion Kinetics for Atoms in Coystals*, Ch. 5, Van Norstrand, Princeton, N. J. (1968).
- 15. A. R. Stokes, "A Numerical Fourier-Analysis Method for the Correction of Widths and Shapes of Lines on X-Ray Powder Photographs", Proc. Phys. Soc., (London) **B61**, 382 (1948).

Abstract—The second harmonic generation in piezoelectric semiconductor are investigated by assuming a parabolic band structure. The second harmonic generation can be found to be expressed in terms of the fundamental. It is pointed out that the amplitude of second harmonic generation is proportional to the square of the amplitude of the fundamental and depends upon the sound velocity for piezoelectric materials. Therefore the intensity of the second harmonic generation is proportional to the square of the intensity of the fundamental. The second harmonic generation in piezoelectric semiconductor is investigated in this paper. The physical situation is that the self-consistent field produced by the interaction of the conduction electrons with the travelling ultrasonic wave contains the second harmonic. Therefore, the interaction of the conduction electrons with the travelling ultrasonic wave can be used to study second harmonic generation. The quantum treatment of optical second harmonic generation has been investigated by several authors.^{1,2} In this paper we investigate second harmonic generation in piezoelectric semiconductor using a quantum treatment which is valid for high frequencies and also for strong magnetic fields. For obtaining the linear and non-linear conductivity tensors, the current density can be expressed in terms of the linear and nonlinear self-consistent fields.^{3,4,5,6} It is assumed that the semiconductor is nondegenerate and the effect of electron scattering on the electron-phonon interaction is neglected. We also limit ourselves to the case where the ultrasonic propagates parallel to a dc magnetic field. It is shown that the amplitude of the